Sensitivity of the backscattering Mueller matrix to particle shape and thermodynamic phase

Ping Yang, Heli Wei, George W. Kattawar, Yong X. Hu, David M. Winker, Chris A. Hostetler, and Bryan A. Baum

The Mueller matrix (M) corresponding to the phase matrix in the backscattering region (scattering angles ranging from 175° to 180°) is investigated for light scattering at a 0.532-μm wavelength by hexagonal ice crystals, ice spheres, and water droplets. For hexagonal ice crystals we assume three aspect ratios (plates, compact columns, and columns). It is shown that the contour patterns of the backscattering Mueller matrix elements other than M_{11}, M_{44}, M_{14}, and M_{41} depend on particle geometry; M_{22} and M_{33} are particularly sensitive to the aspect ratio of ice crystals. The Mueller matrix for spherical ice particles is different from those for nonspherical ice particles. In addition to discriminating between spherical and nonspherical particles, the Mueller matrix may offer some insight as to cloud thermodynamic phase. The contour patterns for large ice spheres with an effective size of 100 μm are substantially different from those associated with small water droplets with an effective size of 4 μm.

OCIS codes: 290.5850, 290.1350, 010.1310, 290.1090.

1. Introduction

We present a theoretical framework involving use of the Mueller matrix to investigate differences between spherical water and ice cloud particles and nonspherical hexagonal ice crystals typically found in clouds ranging from the middle to the upper troposphere. The Mueller matrix approach is explored to improve use of polarimetric backscattering measurements to infer cloud thermodynamic phase and aspects of the cloud particle sphericity. The Mueller matrix is an important parameter in the study of the polarization configuration associated with light-scattering and radiative transfer processes. In fact, the effective Mueller matrix[1] is essentially a matrix Green function for the entire scattering–radiative process. In practice, the 16 Mueller matrix elements can be determined by taking 49 polarimetric measurements at various combinations of input and output analyzer polarization states.[2] An important point to note is that the first three rows and columns of the Mueller matrix involve only linear polarization measurements; however, the fourth row and column mix linear and circular polarization with the exception of the 44 element that involves only circular polarization states. We label the states with a two-letter system; for example, LR would mean that we use a left-circular polarizer (L) for the input state and a right-circular analyzer (R) for the output state. To measure the 44 element, one needs the intensity measurement for the following combinations: $[(LL) + (RR)] - [(RL) + (LR)]$. All the other elements are obtained in a similar way.

Polarimetry is a powerful tool that has been employed in various disciplines as diverse as astronomy and oceanography for many years (see Gehrels[3] and references cited therein). In recent years, there has been an increasing awareness of the benefits associated with use of polarization information in various passive and active remote sensing implementations. For example, Sassen[4] showed the advantages of a lidar polarization technique for retrieving cloud microphysical properties. Polarization anisotropy in lidar multiple scattering from atmospheric clouds was illustrated by Pal and Carswell.[5] In a number of their studies, Kattawar and colleagues (Kattawar and Rakovic[1] and Rakovic *et al.*[6]) demonstrated the

P. Yang (pyang@ariel.met.tamu.edu) and H. Wei are with the Department of Atmospheric Sciences, TAMU 3150, Texas A&M University, College Station, Texas 77843-3150. G. W. Kattawar is with the Department of Physics, TAMU 4242, Texas A&M University, College Station, Texas 77843-4242. Y. X. Hu, D. M. Winker, C. A. Hostetler, and B. A. Baum are with NASA Langley Research Center, Mail Stop 420, Hampton, Virginia 23681.

Received 30 January 2003; revised manuscript received 21 April 2003

0003-6935/03/214389-07$15.00/0

virtues of Mueller matrix imaging for underwater target detection in turbid media. Mishchenko and Sassen[7] showed that the depolarization of lidar returns can be useful to the study of contrail clouds. The sensitivity studies by Hu *et al.*[8,9] demonstrated that passive remote sensing measurements of polarization can be a powerful technique for determining cloud thermodynamic phase. Furthermore, the upcoming NASA Cloud-Aerosol Lidar and Infrared Pathfinder Satellite Observations (CALIPSO, previously named PICASSO–CENA [Pathfinder Instruments for Cloud and Aerosol Spaceborne Observations–Climatologie Etendue des Nuages et des Aerosols][10]) mission, featuring a two-wavelength polarization-sensitive lidar, will provide unprecedented data sets for studying cloud and aerosol particles in the atmosphere by use of a combination of passive and active remote sensing techniques based on polarization information, as articulated by Winker and Wielicki.[10]

Recently, Ben-David[11] formulated and discussed the Mueller matrix associated with the single-order scattering events for various geometric configurations. Once the effective Mueller matrix is known, the computation of the Stokes parameters is straightforward. In this study, we investigate the sensitivity of the contours of the backscattering Mueller matrix to particle shape following the theoretical framework provided by Ben-David.[11] Specifically, we study the backscattering Mueller matrix associated with light scattering at a 0.532-μm wavelength by hexagonal ice crystals, ice spheres, and water droplets. In Section 2 we outline the basic mathematical equations for computing the Mueller matrices. Numerical results are discussed in Section 3. Finally, conclusions of this study are given in Section 4.

2. Mueller Image Associated with Particle Backscattering

To specify the polarization configuration of a radiation beam, the Stokes parameters (I, Q, U, V) are required. The Stokes parameters are defined as follows (van de Hulst[12]):

$$I = < E_{\parallel} E_{\parallel}^{*} > + < E_{\perp} E_{\perp}^{*} >, \tag{1a}$$

$$Q = < E_{\parallel} E_{\parallel}^{*} > - < E_{\perp} E_{\perp}^{*} >, \tag{1b}$$

$$U = < E_{\parallel} E_{\perp}^{*} > + < E_{\parallel}^{*} E_{\perp} >, \tag{1c}$$

$$V = i(< E_{\parallel} E_{\perp}^{*} > - < E_{\parallel}^{*} E_{\perp} >), \tag{1d}$$

where $E_{\parallel}$ and $E_{\perp}$ are, respectively, the parallel and perpendicular components of the electric field specified with respect to a reference plane; the asterisk denotes the complex conjugate; and the brackets denote a temporal average. The polarization features of a radiation beam in terms of the Stokes parameters have been discussed in a number of monographs and texts (e.g., van de Hulst,[12] Chandrasekhar,[13] Bohren and Huffman,[14] Mishchenko *et al.*,[15] and Liou[16]). In the present study we investigate the Mueller matrix associated with the single-order backscattering by ice crystals and water droplets. For simplicity, we assume that nonspherical ice crystals are randomly oriented in space. For randomly oriented particles, having a plane of symmetry, the scattered Stokes parameters are related to their incident counterparts by the phase matrix in the following form (six parameters)[12]:

$$\begin{bmatrix} I_s \\ Q_s \\ U_s \\ V_s \end{bmatrix} = \frac{\sigma_s}{4\pi r^2} \begin{bmatrix} P_{11} & P_{12} & 0 & 0 \\ P_{12} & P_{22} & 0 & 0 \\ 0 & 0 & P_{33} & -P_{43} \\ 0 & 0 & P_{43} & P_{44} \end{bmatrix} \begin{bmatrix} I_i \\ Q_i \\ U_i \\ V_i \end{bmatrix}, \tag{2}$$

where r is the distance between an observer and the scattering particle, and σ_s is the scattering cross section. The scattering phase matrix becomes diagonal for exact backscattering because the elements P_{12} and P_{43} are zero when the scattering angle θ is 180°. Note that the phase function P_{11} in Eq. (2) is normalized so that

$$\frac{1}{2} \int_0^{\pi} P_{11}(\theta) \sin \theta \, d\theta = 1. \tag{3}$$

As shown in Fig. 1, we consider a collimated radiation beam illuminating a thin layer composed of particles along the z-axis direction from below. For simplicity, the particle concentration is assumed to be low (i.e., the optical thickness for the layer is small) so that the backscattered energy is essentially contributed by the first-order scattering events. One method of observing the backscattered Stokes parameters employs use of optical detectors such as a charge-coupled device (CCD) optical array. If such an array was placed on the XOY plane, the backscattered Stokes parameters could be related to the incident Stokes parameters as follows:

$$\begin{bmatrix} I_s(x, y) \\ Q_s(x, y) \\ U_s(x, y) \\ V_s(x, y) \end{bmatrix} = M(x, y) \begin{bmatrix} I_i \\ Q_i \\ U_i \\ V_i \end{bmatrix}, \tag{4}$$

where both the incident and the scattered Stokes parameters need to be specified with a fixed laboratory reference plane. The quantity $M(x, y)$ is an effective Mueller matrix observed at point $R(x, y)$ on the XOY plane, which is a 4 by 4 matrix denoted by

$$M = \begin{bmatrix} M_{11} & M_{12} & M_{13} & M_{14} \\ M_{21} & M_{22} & M_{23} & M_{24} \\ M_{31} & M_{32} & M_{33} & M_{34} \\ M_{41} & M_{42} & M_{43} & M_{44} \end{bmatrix}. \tag{5}$$

For the incident and scattering geometric configuration shown in Fig. 1, we chose the YOZ plane as the laboratory reference plane for specifying the Stokes parameters. For a pixel at point $R(x, y)$, the azimuthal angle of the scattering plane, ROZ, is ϕ (see Fig. 1). Let (I_{iy}, Q_{iy}, U_{iy}, V_{iy}) and (I_{ip}, Q_{ip}, U_{ip}, V_{ip}) be the incident Stokes parameters specified with respect

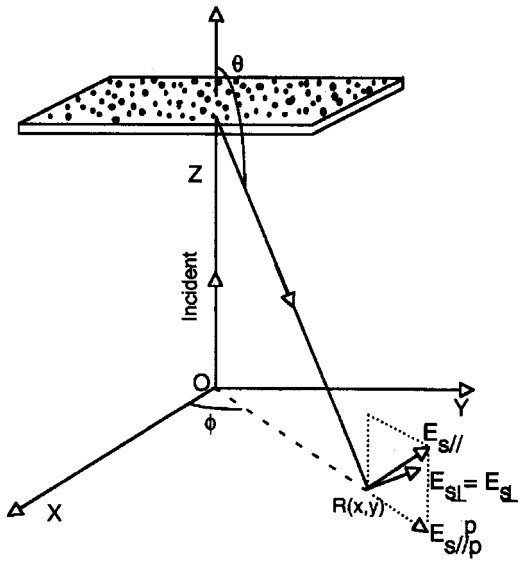

Fig. 1. Incident and scattering geometry for backscattering by a thin layer composed of scattering particles.

where N is the total number of the particles within the scattering volume, i.e., the product of the cross section of the incident beam and the thickness of the scattering layer, and $<\sigma_s>$ is the mean scattering cross section for the particles within the scattering volume.

Let the two components (parallel and perpendicular to the scattering plane) of the scattered field be $E_{s\parallel}$ and $E_{s\perp}$. These two components are associated with the Stokes parameters (I_{sp}, Q_{sp}, U_{sp}, V_{sp}) in Eq. (7). The backscattered electric field has a component parallel to the z axis that will not be measured by a detector placed in the XOY plane (see Fig. 1), as pointed out by Ben-David.[11] From the geometry shown in Fig. 1, the components of the scattered field, after being projected in two directions in the XOY plane, are given by the following transform:

$$\begin{bmatrix} E_{s\perp p} \\ E_{s\parallel p} \end{bmatrix} = \begin{bmatrix} 1 & 0 \\ 0 & \cos(\pi - \theta) \end{bmatrix} \begin{bmatrix} E_{s\perp} \\ E_{s\parallel} \end{bmatrix}. \tag{8}$$

Let (I_{sp}', Q_{sp}', U_{sp}', V_{sp}') be the scattered Stokes parameters associated with $E_{s\perp p}$ and $E_{s\parallel p}$. Using the definition of the Stokes parameters in Eqs. (1a)–(1d), one can derive the relationship

$$\begin{bmatrix} I_{sp}' \\ Q_{sp}' \\ U_{sp}' \\ V_{sp}' \end{bmatrix} = \begin{bmatrix} (\cos^2\theta + 1)/2 & (\cos^2\theta - 1)/2 & 0 & 0 \\ (\cos^2\theta - 1)/2 & (\cos^2\theta + 1)/2 & 0 & 0 \\ 0 & 0 & -\cos\theta & 0 \\ 0 & 0 & 0 & -\cos\theta \end{bmatrix} \begin{bmatrix} I_{sp} \\ Q_{sp} \\ U_{sp} \\ V_{sp} \end{bmatrix}. \tag{9}$$

to the laboratory reference plane YOZ and the scattering plane ROZ, respectively. Note that the field components parallel and perpendicular to the reference plane are $E_\parallel$ and $E_\perp$ in Eqs. (1a)–(1d), respectively. Given the definition of the Stokes parameters, it can be shown that

$$\begin{bmatrix} I_{ip} \\ Q_{ip} \\ U_{ip} \\ V_{ip} \end{bmatrix} = \begin{bmatrix} 1 & 0 & 0 & 0 \\ 0 & \cos 2(\pi/2 - \phi) & \sin 2(\pi/2 - \phi) & 0 \\ 0 & -\sin 2(\pi/2 - \phi) & \cos 2(\pi/2 - \phi) & 0 \\ 0 & 0 & 0 & 1 \end{bmatrix} \times \begin{bmatrix} I_{iy} \\ Q_{iy} \\ U_{iy} \\ V_{iy} \end{bmatrix}. \tag{6}$$

The scattered Stokes parameters specified with respect to the ROZ plane (scattering plane) and observed in the backward hemisphere are given by

$$\begin{bmatrix} I_{sp} \\ Q_{sp} \\ U_{sp} \\ V_{sp} \end{bmatrix} = \frac{N < \sigma_s >}{4\pi r^2} \begin{bmatrix} P_{11} & P_{12} & 0 & 0 \\ P_{12} & P_{22} & 0 & 0 \\ 0 & 0 & P_{33} & -P_{43} \\ 0 & 0 & P_{43} & P_{44} \end{bmatrix} \times \begin{bmatrix} I_{ip} \\ Q_{ip} \\ U_{ip} \\ V_{ip} \end{bmatrix}, \tag{7}$$

The Stokes parameters (I_{sp}', Q_{sp}', U_{sp}', V_{sp}') in Eq. (9) are azimuthally specified with respect to the scattering plane POZ. For polarimetric measurements by detectors placed on and referenced to the XOY plane, the Stokes parameters must be specified with respect to the laboratory reference plane, which is selected as YOZ. The corresponding transformation for the Stokes parameters is given as follows:

$$\begin{bmatrix} I_{sy} \\ Q_{sy} \\ U_{sy} \\ V_{sy} \end{bmatrix} = \begin{bmatrix} 1 & 0 & 0 & 0 \\ 0 & \cos 2(\pi/2 - \phi) & \sin 2(\pi/2 - \phi) & 0 \\ 0 & -\sin 2(\pi/2 - \phi) & \cos 2(\pi/2 - \phi) & 0 \\ 0 & 0 & 0 & 1 \end{bmatrix} \times \begin{bmatrix} I_{sp}' \\ Q_{sp}' \\ U_{sp}' \\ V_{sp}' \end{bmatrix}. \tag{10}$$

With Eqs. (6)–(10), the observed Stokes parameters can be related to the incident Stokes parameters by an effective Mueller matrix in the form of Eq. (4), that is,

$$\begin{bmatrix} I_{sy} \\ Q_{sy} \\ U_{sy} \\ V_{sy} \end{bmatrix} = M \begin{bmatrix} I_{iy} \\ Q_{iy} \\ U_{iy} \\ V_{iy} \end{bmatrix}, \tag{11}$$

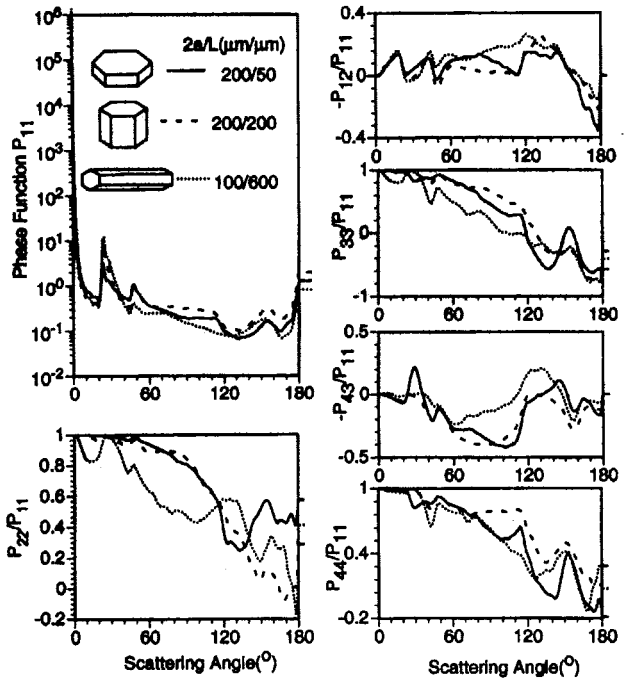

Fig. 2. Nonzero elements of the phase matrix for hexagonal ice crystals with three aspect ratios. Here, L and a are, respectively, the length and the radius of the cylinder circumscribing the ice crystal.

where the effective Mueller matrix is given by

code developed by Wiscombe[19] for the Lorenz–Mie theory is applied for light scattering by spherical water and ice particles.

Figure 2 shows the nonzero elements of phase matrices for hexagonal ice crystals with three aspect ratios, $2a/L = 200/50$ μm (plate), 200/200 μm (compact column), and 100/600 μm (column), where L and a are, respectively, the length and the radius of the cylinder circumscribing the ice crystal. In this study we do not address the details of the phase matrix of hexagonal ice crystals because they have been discussed extensively by Cai and Liou,[20] Takano and Liou,[21] Macke *et al.*,[22] and many others. The size parameters involved in Fig. 2 are large enough to fall within the geometrical-optics regime. For conservative scattering by particles having a large size parameter, the phase matrix is determined by the particle's aspect ratio. The phase matrix is independent of particle dimension except for forward scattering where the magnitude of the Fraunhofer diffraction is size dependent. The primary conclusion to be drawn from Fig. 2 is that the scattering phase matrix is quite sensitive to the particle aspect ratio.

For comparison of nonspherical to spherical particles, we also calculated the phase matrix of ice spheres and spherical water droplets. Substantial phase interference fluctuations are noted in the phase matrix elements for individual spheres (not shown). The integration of individual particle

$$M = \frac{N < \sigma_s >}{4\pi r^2} \begin{bmatrix} 1 & 0 & 0 & 0 \\ 0 & -\cos(2\phi) & \sin(2\phi) & 0 \\ 0 & -\sin(2\phi) & -\cos(2\phi) & 0 \\ 0 & 0 & 0 & 1 \end{bmatrix} \begin{bmatrix} (\cos^2\theta + 1)/2 & (\cos^2\theta - 1)/2 & 0 & 0 \\ (\cos^2\theta - 1)/2 & (\cos^2\theta + 1)/2 & 0 & 0 \\ 0 & 0 & -\cos\theta & 0 \\ 0 & 0 & 0 & -\cos\theta \end{bmatrix}$$

$$\times \begin{bmatrix} P_{11}(\theta) & P_{12}(\theta) & 0 & 0 \\ P_{12}(\theta) & P_{22}(\theta) & 0 & 0 \\ 0 & 0 & P_{33}(\theta) & P_{43}(\theta) \\ 0 & 0 & P_{43}(\theta) & P_{44}(\theta) \end{bmatrix} \begin{bmatrix} 1 & 0 & 0 & 0 \\ 0 & -\cos(2\phi) & \sin(2\phi) & 0 \\ 0 & -\sin(2\phi) & -\cos(2\phi) & 0 \\ 0 & 0 & 0 & 1 \end{bmatrix}. \tag{12}$$

3. Numerical Results and Discussions

For any particular scattering particle, the scattering phase matrix of the scattering particle is required to calculate the effective Mueller matrix. In this study, calculations are performed at a nonabsorptive wavelength of 0.532 μm, at which scattering is essentially conservative and all extinction is due solely to scattering. The complex refractive indices[17] of ice and water at this wavelength are $1.3117 + i2.57 \times 10^{-9}$ and $1.3343 + i1.53 \times 10^{-9}$, respectively. To calculate the scattering phase matrix of hexagonal (i.e., nonspherical) ice crystals, we employ the improved geometrical-optics method developed by Yang and Liou.[18] The computational scattering properties over a particle size distribution tends to smooth out the fluctuations. Following Hansen and Travis,[23] we assume a Gamma size distribution given by

$$n(r) = \frac{N_0 (r_{\text{eff}} V_{\text{eff}})^{(V_{\text{eff}}-1)/V_{\text{eff}}}}{\Gamma[(1 - 2V_{\text{eff}})/V_{\text{eff}}]} r^{(1-3V_{\text{eff}})/V_{\text{eff}}} \times \exp(-r/r_{\text{eff}} V_{\text{eff}}), \tag{13}$$

where N_0 is the total number of the droplets in a unit volume. The quantities r_{eff} and V_{eff} are the effective

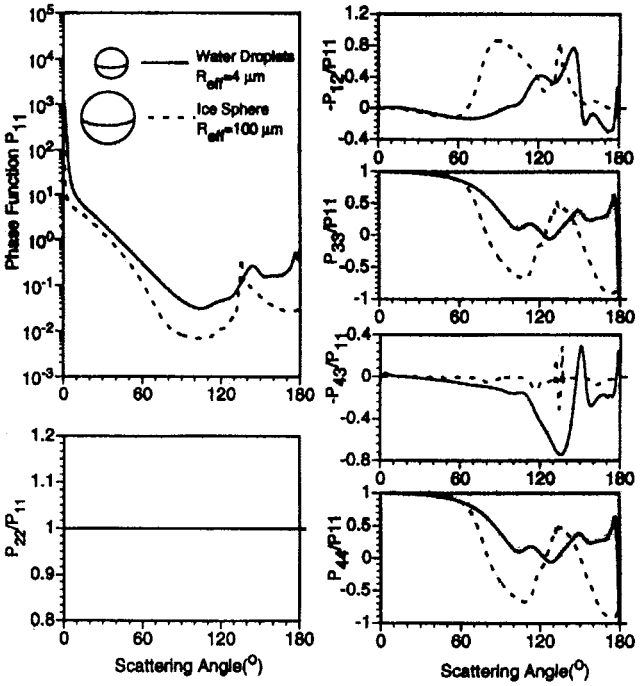

Fig. 3. Nonzero elements of the phase matrix for ice spheres and spherical water droplets.

radius and effective variance that are defined, respectively, as follows:

$$r_{\text{eff}} = \frac{\int_{r_1}^{r_2} r^3 n(r)\mathrm{d}r}{\int_{r_1}^{r_2} r^2 n(r)\mathrm{d}r}, \tag{14}$$

$$V_{\text{eff}} = \frac{\int_{r_1}^{r_2} (r - r_{\text{eff}})^2 r^2 n(r)\mathrm{d}r}{r_{\text{eff}}^2 \int_{r_1}^{r_2} r^2 n(r)\mathrm{d}r}. \tag{15}$$

We assume that $V_{\text{eff}} = 0.1$ in the present study, which corresponds to fair-weather cumulus clouds.[24] For light scattering by spheres, there are only four independent phase matrix elements: P_{11}, P_{12}, P_{33}, and P_{43}. Note that $P_{22} = P_{11}$, $P_{44} = P_{33}$, and $P_{34} = P_{43}$. Figure 3 shows the nonzero phase matrix elements of ice spheres and liquid droplets. Comparing the results shown in Figs. 2 and 3, one can note significant differences for the values of P_{22}/P_{11} for spherical and nonspherical particles. It has been suggested that the deviation of P_{22}/P_{11} from unity value is an index of nonsphericity.[14,15]

Figures 4, 5, and 6 show the contours (images) of each element of the Mueller matrix defined in Eq. (12) for ice column ($2a/L = 100/600$ μm), compact ice crystals ($2a/L = 200/200$ μm), and plate ($2a/L = 200/50$ μm). The Mueller images are observed on a

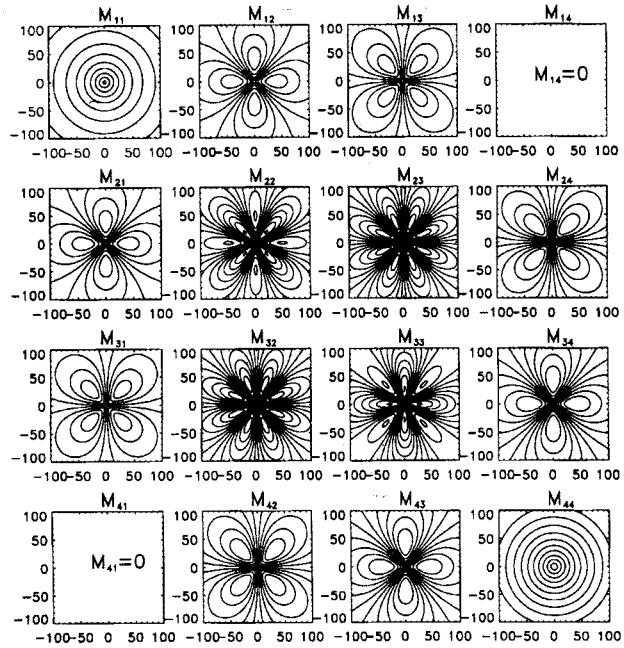

Fig. 4. Contours of the Mueller matrix for backscattering by randomly oriented hexagonal column ice crystals ($2a/L = 100/600$ μm, $R_{\text{eff}} = 113.5$ μm). The X and Y coordinates for each of the Mueller images indicate the positions of the pixels on the image plane (same as in Figs. 5–8).

plane that is perpendicular to the exact backscattering direction. The X and Y coordinates for each of the Mueller images indicate the positions of the pixels on the image plane. In the numerical computations, we assume that the pixel at the center of each

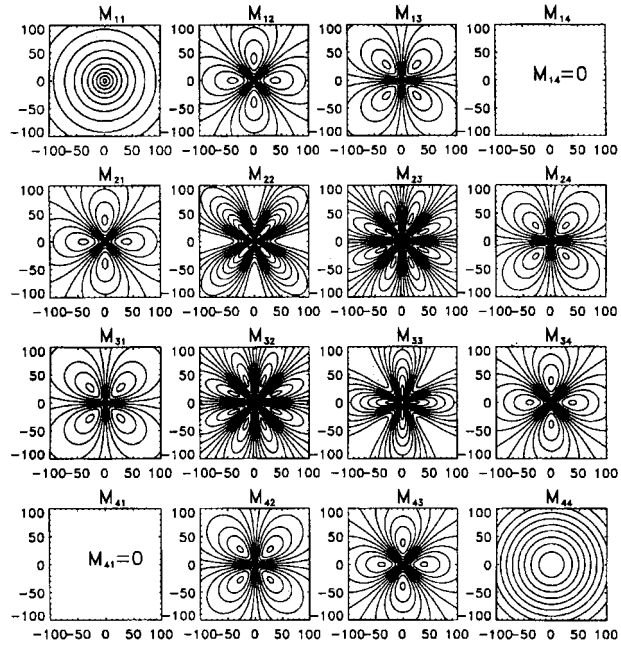

Fig. 5. Contours of the Mueller matrix for backscattering by randomly oriented hexagonal compact ice crystals ($2a/L = 200/200$ μm, $R_{\text{eff}} = 139.1$ μm).

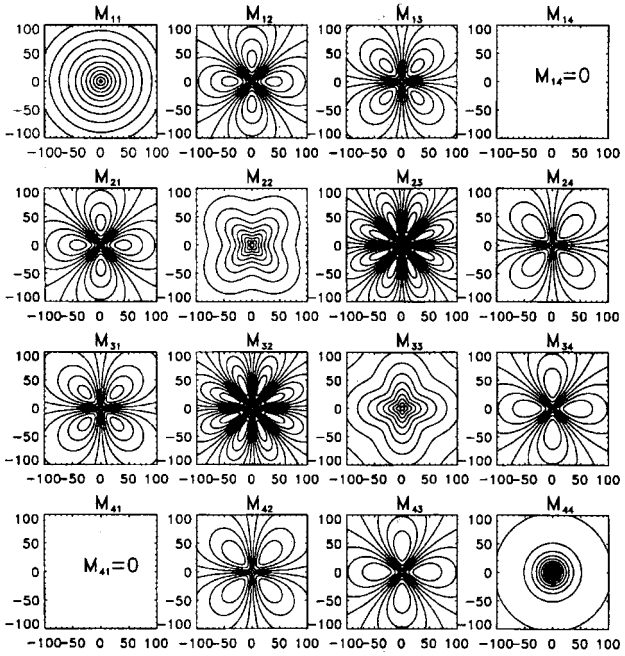

Fig. 6. Contours of the Mueller matrix for backscattering by randomly oriented hexagonal plate ice crystals ($2a/L$ = 200/50 μm, R_{eff} = 58.2 μm).

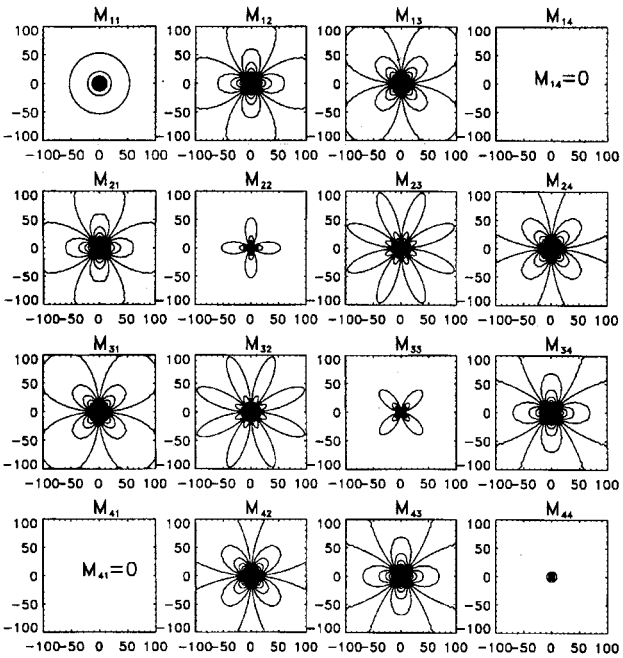

Fig. 7. Contours of the Mueller matrix for backscattering by ice spheres (R_{eff} = 100 μm).

image, i.e., (0,0), corresponds to the exact backscattering direction (i.e., 180°) whereas the corners (±100, ±100) correspond to a 175° scattering angle.

From Figs. 4–6 it is evident that $M_{14} = M_{41} = 0$ regardless of the particle aspect ratio. This result is always true for single scattering from a phase matrix of the form for randomly oriented particles. In addition, the symmetry pattern of Mueller matrix elements can also be noted; for example, the contour patterns for M_{23} and M_{32} are identical. However, it should be pointed out that the signs of the numerical values of M_{ij} and M_{ji} are opposite. Note that the structure and symmetry relationship of the Mueller matrix have been discussed extensively by Hovenier[25] and Hu *et al.*[26] From Figs. 4–6 we note that M_{22} and M_{33} are quite sensitive to the aspect ratio of ice crystals. For the Mueller matrix, the 3 × 3 elements in the upper left corner are associated only with a linear polarization configuration. The linear polarization is easier to quantify by laboratory or field measurements than is circular polarization. Thus the sensitivity of M_{22} and M_{33} to the particle aspect ratio may be useful for determining particle morphology.

Figure 7 shows the contours of the Mueller matrix for ice spheres with an effective size of 100 μm. The Mueller matrix for ice spheres is significantly different from that associated with hexagonal ice crystals. We also note that the patterns shown for ice spheres are similar to those shown by Rakovic *et al.*,[6] who compared experimental and theoretical results for the Mueller matrix associated with polystyrene spheres in deionized water.

Figure 8 shows the contours of the Mueller matrix for water droplets with an effective size of 4 μm. Comparing Figs. 6 and 7, one can see that the pattern of the Mueller matrix contours for small water droplets and large ice spheres are different. The results for water droplets are also different from those for hexagonal ice crystals. Thus, by measuring the Muller matrix associated with cloud particles, one can differentiate the thermodynamic phase of clouds

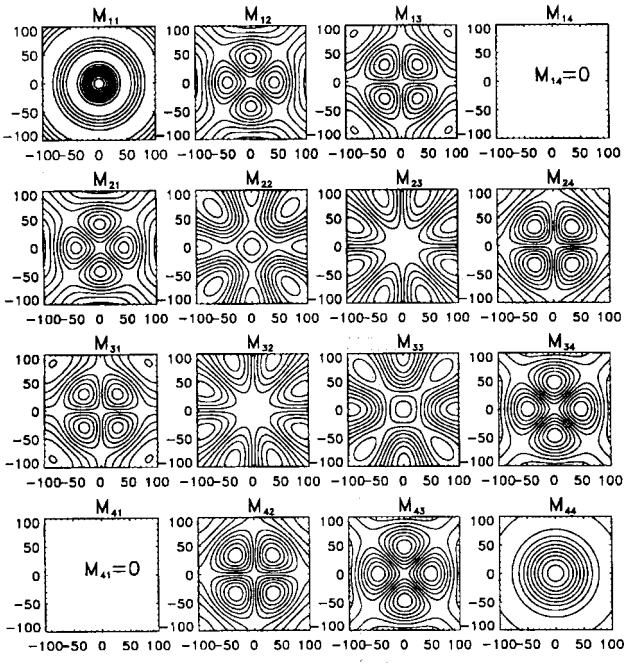

Fig. 8. Contours of the Mueller matrix for backscattering by spherical water droplets (R_{eff} = 4 μm).

because of the different characteristics of the Muller matrix for ice particles and water droplets.

4. Conclusions

Following Ben-David,[11] we have formulated the backscattering Mueller matrix associated with a thin layer of ice crystals or water droplets. An improved geometrical-optics model is employed to calculate all the nonzero elements of the phase matrix for hexagonal ice crystals that are assumed to be randomly oriented in space. The phase matrix of ice spheres or water droplets are computed from the Lorenz–Mie theory with an inclusion of a Gamma size distribution. We calculate the backscattering Mueller matrix that corresponds to scattering angles between 175° and 180°.

For hexagonal ice crystals, three aspect ratios (plates, compact columns, and columns) are used to calculate the Mueller matrix. We show that the Mueller matrix elements other than M_{41}, M_{14}, M_{11}, and M_{44} depend on particle geometry. In particular, we find that M_{22} and M_{33} are quite sensitive to the particle aspect ratio.

We explore the ability of the backscattering Mueller matrix to discriminate between ice and water particles. Our results show substantial differences in the Mueller matrix between large ice spheres and small liquid droplets. In addition, the contours of the Mueller matrix are also significantly different for ice spheres and nonspherical ice crystals. Based on our results, we conclude that measurements based on the Mueller matrix could be used to discriminate between ice and water clouds.

This research has been supported by the NASA CALIPSO project, NASA Radiation Science Program managed by Donald Anderson (NAG5-11374), and by the U.S. Office of Naval Research under contract N00014-02-1-0478.

References

1. G. W. Kattawar and M. J. Rakovic, "Virtues of Mueller matrix imaging for underwater target detection," Appl. Opt. **38,** 6431–6438 (1999).
2. B. D. Cameron, M. J. Rakovic, M. Mehrubeoglu, G. W. Kattawar, S. Rastegar, L. V. Wang, and G. L. Cote, "Measurement and calculation of the two-dimensional backscattering Mueller matrix of a turbid medium," Opt. Lett. **23,** 485–487 (1998).
3. T. Gehrels, ed., *Planets, Stars and Nebulae* (University of Arizona, Tucson, Ariz,, 1974).
4. K. Sassen, "The polarization lidar technique for cloud research: a review and current assessment," Bull. Am. Meteorol. Soc. **72,** 1848–1866 (1991).
5. S. R. Pal and A. I. Carswell, "Polarization anisotropy in lidar multiple scattering from atmospheric clouds," Appl. Opt. **24,** 3464–3471 (1985).
6. M. J. Rakovic, G. W. Kattawar, B. D. Cameron, M. Mehrubeoglu, S. Rastegar, L. V. Wang, and G. L. Cot, "Light backscattering polarization patterns from turbid media: theory and experiment," Appl. Opt. **38,** 3399–3408 (1999).
7. M. I. Mishchenko and K. Sassen, "Depolarization of lidar returns by small ice crystals: an application to contrails," Geophys. Res. Lett. **25,** 309–312 (1998).
8. Y. X. Hu, D. Winker, P. Yang, B. A. Baum, L. Poole, and L. Vann, "Identification of cloud phase from PICASSO-CENA lidar depolarization: a multiple scattering sensitivity study," J. Quant. Spectrosc. Radiat. Transfer **70,** 569–579 (2001).
9. Y. X. Hu, P. Yang, B. Lin, and C. Hostetler, "Discriminating between spherical and non-spherical scatters with lidar using circular component: a theoretical study," J. Quant. Spectrosc. Radiat. Transfer **79–80,** 757–764 (2003).
10. D. M. Winker and B. A. Wielicki, "The PICASSO-CENA mission," in *Sensors, Systems, and Next-Generation Satellites III,* H. Fujisada and J. B. Lurie, eds., Proc. SPIE **3870,** 26–36 (1999).
11. A. Ben-David, "Mueller matrices and information derived from linear polarization lidar measurements: theory," Appl. Opt. **37,** 2448–2463 (1998).
12. H. C. van de Hulst, *Light Scattering by Small Particles* (Wiley, New York, 1957).
13. S. Chandrasekhar, *Radiative Transfer* (Oxford U. Press, London, 1950).
14. C. F. Bohren and D. R. Huffman, *Absorption and Scattering of Light by Small Particles* (Wiley, New York, 1983).
15. M. I. Mishchenko, L. D. Travis, and A. A. Lacis, *Scattering, Absorption, and Emission of Light by Small Particles* (Cambridge U. Press, Cambridge, UK, 2002).
16. K. N. Liou, *An Introduction to Atmospheric Radiation*, 2nd ed. (Academic, San Diego, Calif., 2002).
17. S. G., Warren, "Optical constants of ice from the ultraviolet to the microwave," Appl. Opt. **23,** 1206–1225 (1984).
18. P. Yang and K. N. Liou, "Geometric-optics–integral-equation method for light scattering by nonspherical ice crystals," Appl. Opt. **35,** 6568–6584 (1996).
19. W. J. Wiscombe, "Improved Mie scattering algorithms," Appl. Opt. **19,** 1505–1509 (1980).
20. Q. M. Cai and K. N. Liou, "Theory of polarized light scattering by hexagonal ice crystals," Appl. Opt. **21,** 3569–3580 (1982).
21. Y. Takano and K. N. Liou, "Solar radiative transfer in cirrus clouds. I. Single-scattering and optical properties of hexagonal ice crystals," J. Atmos. Sci. **46,** 3–19 (1989).
22. A. Macke, J. Muller, and E. Rascke, "Single-scattering properties of atmopsheric crystals," J. Atmos. Sci. **53,** 2813–2825 (1996).
23. J. E. Hansen and L. D. Travis, "Light scattering in planetary atmospheres," Space Sci. Rev. **16,** 527–610 (1974).
24. M. D. King, "Determination of the scaled optical thickness of clouds from reflected solar radiation measurements," J. Atmos. Sci. **44,** 1734–1751 (1987).
25. J. W. Hovenier, "Structure of a general pure Mueller matrix," Appl. Opt. **33,** 8318–8324 (1994).
26. C. R. Hu, G. W. Kattawar, M. E. Parkin, and P. Herb, "Symmetry theorems on the forward and backward scattering Mueller matrix for light scattering from a nonspherical dielectric scatter," Appl. Opt. **26,** 4159–4173 (1987).